AEM
Journals.ASM.org

Focused Directed Evolution of Aryl-Alcohol Oxidase in *Saccharomyces cerevisiae* by Using Chimeric Signal Peptides

Javier Viña-Gonzalez,[a] David Gonzalez-Perez,[a] Patricia Ferreira,[b] Angel T. Martinez,[c] Miguel Alcalde[a]

Department of Biocatalysis, Institute of Catalysis, CSIC, Madrid, Spain[a]; Departamento de Bioquímica y Biología Molecular y Celular, Facultad de Ciencias, Universidad de Zaragoza, and Instituto de Biocomputación y Física de Sistemas Complejos, Zaragoza, Spain[b]; Centro de Investigaciones Biológicas, CSIC, Madrid, Spain[c]

Aryl-alcohol oxidase (AAO) is an extracellular flavoprotein that supplies ligninolytic peroxidases with H_2O_2 during natural wood decay. With a broad substrate specificity and highly stereoselective reaction mechanism, AAO is an attractive candidate for studies into organic synthesis and synthetic biology, and yet the lack of suitable heterologous expression systems has precluded its engineering by directed evolution. In this study, the native signal sequence of AAO from *Pleurotus eryngii* was replaced by those of the mating α-factor and the K_1 killer toxin, as well as different chimeras of both prepro-leaders in order to drive secretion in *Saccharomyces cerevisiae*. The secretion of these AAO constructs increased in the following order: preproα-AAO > preαproK-AAO > preKproα-AAO > preproK-AAO. The chimeric preαproK-AAO was subjected to focused-directed evolution with the aid of a dual screening assay based on the Fenton reaction. Random mutagenesis and DNA recombination was concentrated on two protein segments (Met[α1]-Val109 and Phe392-Gln566), and an array of improved variants was identified, among which the FX7 mutant (harboring the H91N mutation) showed a dramatic 96-fold improvement in total activity with secretion levels of 2 mg/liter. Analysis of the N-terminal sequence of the FX7 variant confirmed the correct processing of the preαproK hybrid peptide by the KEX2 protease. FX7 showed higher stability in terms of pH and temperature, whereas the pH activity profiles and the kinetic parameters were maintained. The Asn91 lies in the flavin attachment loop motif, and it is a highly conserved residue in all members of the GMC superfamily, except for *P. eryngii* and *P. pulmonarius* AAO. The *in vitro* involution of the enzyme by restoring the consensus ancestor Asn91 promoted AAO expression and stability.

Aryl-alcohol oxidase (AAO; EC 1.1.3.7) is a flavoenzyme of the GMC (glucose-methanol-choline) oxidoreductase superfamily, the members of which share a N-terminal FAD-binding domain containing the canonical ADP-binding motif. Secreted by several white-rot fungi, this monomeric flavoprotein plays an essential role in natural lignin degradation (1). Accordingly, AAO oxidizes lignin-derived compounds and aromatic fungal metabolites, releasing H_2O_2 that is required by ligninolytic peroxidases to attack the plant cell wall (2). Moreover, the H_2O_2 produced by AAO is an efficient vehicle to generate highly reactive hydroxyl radicals through the Fenton reaction ($Fe^{2+} + H_2O_2 \rightarrow OH^{\cdot} + OH^{-} + Fe^{3+}$), such that $OH^{\cdot}$ can act as a diffusible electron carrier to depolymerize plant polymers. AAO oxidizes a variety of aromatic benzyl (and some aliphatic polyunsaturated) alcohols to the corresponding aldehydes. In addition, AAO participates in the oxidation of aromatic aldehydes to the corresponding acids and also has activity on furfural derivatives (3).

The past few years have witnessed an intense effort to discern the basis and mechanism of action underlying AAO catalysis (3–10). The AAO catalytic cycle involves dehydrogenative oxidation mediated by two half-reactions: (i) the reductive half-reaction in which the donor alcohol is two-electron oxidized by the FAD cofactor, the latter receiving one of the alcohol's α-Hs through a hydride transfer process that yields the aldehyde product and the reduced flavin, and (ii) the oxidative half-reaction, in which O_2 is two-electron reduced by the FAD, releasing H_2O_2 and the reoxidized flavin (5).

Directed molecular evolution is by far the best strategy currently available to design enzymes to industrial standards (11–14). However, AAO has not been subjected to directed evolution, probably due to the lack of appropriate functional expression systems. Indeed, AAO has only been heterologous expressed in *Aspergillus nidulans* (15), an unsuitable host for directed evolution experiments (16), and in *Escherichia coli* after the *in vitro* refolding of inclusion bodies, an approach incompatible with directed evolution campaigns (17).

In the present study, the native signal peptide of AAO was replaced by two different signal sequences to drive its functional expression in *Saccharomyces cerevisiae*: (i) the signal prepro-leader of the mating α-factor of *S. cerevisiae*, which has been used widely to evolve different ligninases (18–23), and (ii) the signal prepro(δ)-leader and the γ-spacer segment of the K_1 killer toxin, which have been seen to be useful in boosting β-lactamase secretion in yeast (24, 25). For the first time, chimeric versions of these leaders were designed by combining the different pre- and pro-regions, and these constructs were subjected to conventional and focused-directed evolution using a very sensitive dual high-throughput screening (HTS) assay based on the Fenton reaction. The best mutant identified dramatically improved the total activ-

Received 12 June 2015 **Accepted** 3 July 2015

Accepted manuscript posted online 10 July 2015

Citation Viña-Gonzalez J, Gonzalez-Perez D, Ferreira P, Martinez AT, Alcalde M. 2015. Focused directed evolution of aryl-alcohol oxidase in *Saccharomyces cerevisiae* by using chimeric signal peptides. Appl Environ Microbiol 81:6451–6462. doi:10.1128/AEM.01966-15.

Editor: A. A. Brakhage

Address correspondence to Miguel Alcalde, malcalde@icp.csic.es.

Supplemental material for this article may be found at http://dx.doi.org/10.1128/AEM.01966-15.

doi:10.1128/AEM.01966-15

ity and stability being readily secreted by yeast. Indeed, this active, highly stable and soluble AAO variant is a promising point of departure for new engineering goals.

MATERIALS AND METHODS

All chemicals were of reagent-grade purity. Ferrous ammonium sulfate, xylenol orange, sorbitol, benzyl alcohol, *p*-methoxybenzyl alcohol, veratryl (3,4-dimethoxybenzyl) alcohol, 2,4-hexadien-1-ol, ABTS [2,2′azino-bis(3-ethylbenzthiazolinesulfonic acid)], horseradish peroxidase (HRP), *Taq* polymerase, and a yeast transformation kit were purchased from Sigma (Madrid, Spain). Zymoprep yeast plasmid miniprep, yeast plasmid miniprep kit I, and a Zymoclean gel DNA recovery kit were obtained from Zymo Research (Orange, CA). Restriction enzymes BamHI and XhoI were from New England BioLabs (Hertfordshire, United Kingdom). I-Proof high-fidelity DNA polymerase was from Bio-Rad (USA). The episomal shuttle vector pJRoC30 was from the California Institute of Technology (Caltech) and plasmids pRE1219 and pJRoC30-δγN2C1 were kindly donated by S. Camarero (CIB-CSIC, Madrid, Spain). *E. coli* XL2-Blue competent cells were from Stratagene (La Jolla, CA), whereas the protease-deficient *S. cerevisiae* strain BJ5465 (MATa *ura3-52 trp1 leu2Δ1 his3Δ200 pep4*::*HIS3 prb1Δ1.6R can1 GAL*) was obtained from LGC Promochem (Barcelona, Spain).

Culture media. Minimal medium SC contained 100 ml of 6.7% (wt/vol) sterile yeast nitrogen base, 100 ml of a 19.2-g/liter sterile yeast synthetic dropout medium supplement without uracil, 100 ml of sterile 20% (wt/vol) raffinose, 700 ml of sterile double-distilled H_2O (sddH_2O), and 1 ml of chloramphenicol at 25 g/liter. YP medium contained 10 g of yeast extract, 20 g of peptone, and ddH_2O to 650 ml, whereas YPD medium also contained 20% (wt/vol) glucose. AAO expression medium contained 144 ml of 1.55× YP, 13.4 ml of 1 M KH_2PO_4 (pH 6.0) buffer, 22.2 ml of 2% (wt/vol) galactose, 0.222 ml of chloramphenicol at 25 g/liter, and ddH_2O to 200 ml. Luria broth (LB) medium contained 10 g of sodium chloride, 5 g of yeast extract, 10 g of peptone, 1 ml of ampicillin at 100 mg/ml, and ddH_2O to 1 liter.

Fusion genes and signal chimeric leaders. AAO mature protein was fused both to the α-factor prepro-leader (preproα-AAO, construct i) and to the prepro(δ)-γ regions of the prepro-toxin K_1 killer (preproK-AAO, construct ii). In addition, two chimeric signal peptides were constructed and attached to the AAO: the α-factor pre-leader fused to the γ segment of the K_1 killer toxin (preαproK-AAO, construct iii) and the prepro(δ)-signal sequence of the K_1 killer toxin fused to the α-factor pro-leader (preKproα-AAO, construct iv). The design of overlapping areas of ~40 bp between adjacent fragments allowed the *in vivo* fusion of the different genetic elements using the *S. cerevisiae* homologous recombination machinery.

AAO was amplified from pflag1AAO vector (17) using oligonucleotide sense AAO/N-ter primer (5′-GCCGATTTTGACTACGTTGTCGTCG-3′) and oligonucleotide antisense AAO/C-ter/pJRo-overhang primer (5′-CATAACTAATTACATGATGCGGCCCTCTAGATGCATGCTCGAGCGGCCGCCTACTGATCAGCCTTGATAAGATCGGCT-3′; the overhang for pJRoC30 is underlined). The α-factor prepro-leader (89 residues, including the STE13 cleavage site EAEA) was obtained from pJRoC30-αVP (20) using oligonucleotide sense RMLN primer (5′-CCTCTATACTTTAACGTCAAGG-3′) and oligonucleotide antisense αC-ter/AAO-overhang primer (5′-CCGCGTTCCCCGCCCCGACGACAACGTAGTCAAAATCGGCAGCTTCAGCCTCTCTTTTCTC-3′; the overhang for AAO is underlined). The preα fragment, used to create preαproK-AAO, was amplified from pJRoC30-αVP with oligonucleotide sense RMLN and oligonucleotide antisense preαC-ter/proK-overhang (5′-AGTCGTTAGCTGGGAGTATACTAATACCATGTTCATTTAAGTTGACTGGAGCAGCTAATG-3′; the overhang for the proK is underlined) primers; this fragment was designed to include the 19 residues of the α-pre-leader plus the first four residues—APVN—of the α-pro-leader. The proα fragment (66 residues and the STE13 cleavage site) used to create preKproα-AAO was obtained from pJRoC30-αVP with the oligonucleotide sense proα/N-ter primer (5′-GCTCCAGTCAACACTACAAC-3′) and the oligonucleotide antisense αC-ter/AAO-overhang. Prepro(δ)-leader from the K_1 killer toxin, used as the preK-leader (47 residues long, including the C-terminal EAP acid environment) with different overhangs (for subsequent assembly in yeast to give rise to different chimeras), was obtained from two independent PCRs from plasmid pRE1219, which contains the prepro(δ) region (1 to 44 residues) and the alpha-toxin subunit (45 to 149 residues): (i) to be fused in preproK-AAO with the oligonucleotide sense primer preKN-ter/pJRo-overhang (5′-TATACTTTAACGTCAAGGAGAAAAAACTATAGGATCATAGGATCCATGACGAAGCCAACCCAAGTATTA-3′; the overhang for pJRoC30 is underlined) and the oligonucleotide antisense primer preKC-ter/proK-overhang (5′-AGTCGTTAGCTGGGAGTATACTAATACCATGTTCATTTAACGGCGCTTCACGTTTTAGTAATGACACTGGT-3′; the overhang for proK is underlined) and (ii) with preKN-ter/pJRo-overhang as the oligonucleotide sense primer and preKC-ter/proα-overhang (5′-TTTGTGCCGTTTCATCTTCTGTTGTAGTGTTGACTGGAGCCGGCGCTTCACGTTTTAGTAATGACACTGGT-3′; the overhang for proα is underlined) as the antisense primer to be part of the preKproα-AAO. The truncated γ-spacer-segment from the K_1 killer toxin (64 residues), the proK segment in both preproK-AAO and preαproK-AAO, was obtained from pJRoC30-δγN2C1 with the oligonucleotide sense proKN-ter primer (5′-TTAAATGAACATGGTATTAGTATACTCCCA-3′) and the antisense primer proKC-ter/AAO-overhang (5′-CCGCGTTCCCCGCCCCGACGACAACGTAGTCAAAATCGGCACGCTTGGCCACTGCTGGAAT-3′; the overhang for AAO is underlined).

pJRoC30 was linearized with BamHI and XhoI. PCRs were performed in a final volume of 50 μl containing a 250 nM concentration of each primer, 10 ng of template, deoxynucleoside triphosphates (dNTPs) at 200 μM each, 3% (vol/vol) dimethyl sulfoxide (DMSO), and 0.02 U of iProof high-fidelity polymerase/liter. The amplification reactions were carried out in a thermal cycler Mycycler (Bio-Rad). The PCR cycles were as follows: 98°C for 30 s (1 cycle); 98°C for 10 s, 50°C for 25 s, and 72°C for 60 s (28 cycles); and 72°C for 10 min (1 cycle). PCR fragments and the linearized vector were loaded onto a preparative agarose gel (0.75% [wt/vol]) and purified using a Zymoclean gel DNA recovery kit. PCR products (400 ng of each) were mixed with the linearized vector (100 ng; PCR product/vector ratio of 4:1) and transformed in yeast (yeast transformation kit), promoting the recombination and cloning *in vivo*. Transformed cells were plated in SC (synthetic complete) dropout plates, followed by incubation for 3 days at 30°C; individual clones were fermented in 96-well plates and screened for AAO activity. For each positive construct, the plasmids were extracted and sequenced. Fusions were retransformed into yeast and fermented in 100-ml flasks while monitoring cell growth and activity (using HRP-ABTS and FOX [ferrous oxidation by xylenol orange] assays [see below]) over time.

Focused-directed AAO evolution. All of the PCR products were cleaned, concentrated, loaded onto a low melting-point preparative agarose gel (0.75% [wt/vol]) and purified using a Zymoclean gel DNA recovery kit before being cloned into pJRoC30. The plasmid was linearized with BamHI and XhoI. pJRoC30-preαproK-AAO variant was used as DNA template for focused random mutagenesis. The preαproK-AAO fusion was split into three different segments for MORPHING (Mutagenic Organized Recombination Process by Homologous *IN vivo* Grouping) (26). Amplified by PCR, each fragment included homologous overlapping overhangs of ~50 bp so that the whole gene could be reassembled *in vivo* by transformation into *S. cerevisiae*. Mutagenic regions M-I and M-II (590 and 528 bp, respectively, excluding the recombination areas) were subjected to *Taq*/$MnCl_2$ amplification, and the remaining segment (844 bp) was amplified by high-fidelity PCR. To adjust the mutagenic loads, small mutant libraries (around 500 clones each) were created with equal concentrations of DNA template and different $MnCl_2$ concentrations (0.025, 0.05, and 0.01 mM combining both segments and with 0.05 mM in segment M-I and 0.025 mM in segment M-II). The percentage of inactive clones (with <10% of the parent activity) was calculated to estimate mutational loads. Four mutant libraries were created. Two mutagenic librar-

ies (~1,000 clones each) were prepared targeting segment M-I or segment M-II independently for random mutagenesis. The third library (~1,000 clones, library M-I-II) was constructed by assembling mutagenic segments (M-I and M-II) flanking a nonmutagenic amplification in the middle of the gene. Finally, the whole preαproK-AAO fusion was subjected to *Taq*/$MnCl_2$ amplification (library M-IV), adjusting the mutational rate to 1 to 3 mutations per gene (~2,000 clones). Concentrations of 0.05 and 0.01 mM $MnCl_2$ were used for MORPHING and full gene random mutagenesis, respectively.

(i) Mutagenic PCR of targeted segments. Reaction mixtures were prepared in a final volume of 50 μl containing DNA template (0.92 ng/μl), 90 nM oligonucleotide sense primer (RMLN for segment M-I and AAOMBP [5′-AACTCTGCTCATTGGGAGACCATCT-3′] for segment M-II), 90 nM reverse primer (AAO92C [5′-CCCAGTTCCATCCTTCAT CGCCA-3′] for segment M-I and RMLC [5′-GGGAGGGCGTGAATGT AAGC-3′] for segment M-II), 0.3 mM dNTPs (0.075 mM each), 3% (vol/vol) DMSO, 1.5 mM $MgCl_2$, increasing concentrations of $MnCl_2$ (0.025, 0.05, and 0.1 mM), and 0.05 U of *Taq* DNA polymerase/μl. Mutagenic PCRs parameters were as follows: 95°C for 2 min (1 cycle); 95°C for 45 s, 50°C for 45 s, and 74°C for 45 s (28 cycles); and 74°C for 10 min (1 cycle).

(ii) High-fidelity PCR. Reaction mixtures were prepared in a final volume of 50 μl containing DNA template (0.2 ng/μl), 250 nM oligonucleotide sense HFF (5′-TTCGATCGCTATGCGGCTGTCAC-3′), and 250 nM oligonucleotide antisense HFR (5′-GGGTGGAACCATTGGTTG GAAAAG-3′). High-fidelity PCRs were performed using the following parameters: 98°C for 30 s (1 cycle); 98°C for 10 s, 55°C for 25 s, and 72°C for 45 s (28 cycles); and 72°C for 10 min (1 cycle).

(iii) Whole-gene reassembly. The whole gene was cloned and recombined *in vivo* by transformation into *S. cerevisiae*. PCR products were mixed in equimolar amounts (400 ng) and transformed with linearized plasmid (200 ng) into chemically competent cells. Transformed cells were plated on SC dropout plates and incubated for 3 days at 30°C. Colonies containing the whole autonomously replicating vector were picked and screened for activity.

HTS assay. Individual clones were picked and cultured in sterile 96-well plates containing 50 μl of minimal medium (SC). In each plate, column 6 was inoculated with the parental type (internal standard) and well H1 with URA3$^-$ *S. cerevisiae* cells (negative control). Plates were sealed to prevent evaporation and incubated at 30°C, 225 rpm, and 80% relative humidity in a humidity shaker (Minitron-INFORS; Biogen, Spain). After 48 h, 160 μl of expression medium was added to each well, followed by culture for an additional 48 h. Finally, 20-μl portions of the supernatants were screened for activity with the FOX and HRP-ABTS assays using veratryl or *p*-methoxybenzyl alcohol as the substrate as described below. One unit of AAO activity is defined as the amount of enzyme that converts 1 μmol of alcohol to aldehyde with the stoichiometric formation of H_2O_2 per min under the reaction conditions.

Chemical (direct) FOX assay. Aliquots of 20 μl of yeast supernatants were transferred with liquid handler robotic station Freedom EVO (Tecan, Männedorf, Switzerland) and incubated with 20 μl of substrate (2 mM *p*-methoxybenzyl alcohol or 10 mM veratryl alcohol in 100 mM phosphate buffer [pH 6.0]) for 30 min at room temperature, and then 160 μl of FOX reagent was added with a Multidrop Combi-Reagent dispenser (Thermo Scientific, Waltham, MA) to assess the AAO H_2O_2 production [final concentration of FOX mixture in the well: 100 μM xylenol orange, 250 μM $Fe(NH_4)_2(SO_4)_2$, and 25 mM H_2SO_4] (27). Plates were recorded in endpoint mode at 560 nm using a spectrophotometer SpectraMax 384 Plus (Molecular Devices, Sunnyvale, CA); it required ~20 min of incubation to develop an intense and stable colorimetric response. The relative activities were calculated from the difference between the absorbance value after incubation to that of the initial measurement normalized to the parental type for each plate. To enhance method sensitivity, several additives may be added to the reagent, such as organic cosolvents (DMSO, ethanol, and methanol) or sorbitol (28). In our case, the response was amplified by adding a final concentration of 100 mM sorbitol, which acts as chain amplifier generating additional ferric ions to increase the response of the method (29). The assay was validated by determining the coefficient of variance, the linearity of the response and the detection limit. The detection limit was calculated by the blank determination method on a 96-well plate with triplicate standards (0, 0.5, 1, 1.5, 2, 2.5, 3, and 4 μM H_2O_2) and several portions of supernatants from *S. cerevisiae* URA3$^-$ lacking plasmid (30). FOX signal stability was tested with different H_2O_2 concentrations (0, 2, 4, 6, 8, 10, 15, and 18 μM) for 300 min at 24°C.

Enzymatic (indirect) HRP-ABTS assay. Aliquots of 20 μl of yeast supernatants were added to 180 μl of HRP-ABTS reagent (final concentrations of HRP-ABTS reagent in the well: 1 mM *p*-methoxybenzyl alcohol or 5 mM veratryl alcohol, 2.5 mM ABTS, 1 μg of HRP/ml in 100 mM phosphate buffer [pH 6.0]) dispensed with a Multidrop Combi-Reagent dispenser. The plates were incubated at room temperature and measured in endpoint or kinetic mode at 418 nm ($\varepsilon_{ABTS^{\cdot+}} = 36{,}000\ M^{-1}\ cm^{-1}$).

The dual HTS assay incorporated two consecutive rescreenings to rule out the selection of false positives.

(i) First rescreening. Aliquots of 5 μl of the best clones of the screening were transferred to new sterile 96-well plates with 50 μl of minimal medium per well. Columns 1 and 12 plus rows A and H were not used to prevent the appearance of false positives. After 24 h of incubation at 30°C and 225 rpm, 5-μl portions were transferred to the adjacent wells, followed by further incubation for 24 h. Finally, 160 μl of expression medium was added, and the plates were incubated for 48 h. Accordingly, each mutant was grown in four independent wells. The parental type was subjected to the same procedure (lane D, wells 7 to 11). Plates were assessed according to the same HTS protocol of the screening described above.

(ii) Second rescreening. An aliquot from the best clones from the first rescreening was inoculated in 3 ml of YPD medium, followed by incubation at 30°C for 24 h at 225 rpm. The plasmids from these cultures were recovered with a Zymoprep yeast plasmid miniprep kit I. Since the product of the Zymoprep was impure and the DNA extracted was very low concentrated, the shuttle vectors were transformed into supercompetent *E. coli* XL2-Blue cells and plated onto LB-ampicillin (LB-amp) plates. Single colonies were selected to inoculate 5 ml of LB-amp medium and incubated overnight at 37°C and 225 rpm. The plasmids from the best mutants and the parental type were extracted (NucleoSpin plasmid kit) and transformed into *S. cerevisiae*. Five colonies for each mutant were picked and rescreened as described above.

AAO production and purification. (i) Production of recombinant AAO variants in *S. cerevisiae*. A single colony from the *S. cerevisiae* clone containing the AAO fusion gene was picked from a SC dropout plate, inoculated in SC medium (20 ml) and incubated for 48 h at 30°C and 220 rpm (Minitron-INFORS, Biogen Spain). An aliquot of cells was removed and used to inoculate minimal medium (100 ml) in a 500-ml flask (optical density at 600 nm [OD_{600}] = 0.25). The cells completed two growth phases (6 to 8 h; OD_{600} = 1), and then expression medium (900 ml) was inoculated with the preculture (100 ml; OD_{600} of 0.1). After incubation for 72 h at 25°C and 220 rpm (maximal AAO activity; OD_{600} = 25 to 30), the cells were recovered by centrifugation at 4,500 rpm and 4°C (Avanti J-E centrifuge; Beckman Coulter, Inc., Brea, CA), and the supernatant was double filtered (using both a glass membrane filter and a nitrocellulose membrane [0.45-μm pore size]).

(ii) Purification of AAO mutant. AAO (FX7 variant) was purified by FPLC (ÄKTA purifier; GE Healthcare, United Kingdom). The crude extract was concentrated and dialyzed in 20 mM piperazine buffer (buffer P [pH 5.5]) by tangential ultrafiltration (Pellicon; Millipore, Temecula, CA) through a 10-kDa-pore-size membrane (Millipore) by means of a peristaltic pump (Masterflex Easy Load; Cole-Parmer, Vernon Hills, IL). The sample was filtered and loaded onto a weak anion-exchange column (HiTrap Q FF; GE Healthcare) preequilibrated with buffer P and coupled to the ÄKTA purifier system. The proteins were eluted with a linear gradient of buffer *P* + 1 M NaCl in two phases at a flow rate of 1 ml/min: from 0 to 50% in 15 min and from 50 to 100% in 2 min. Fractions with AAO activity

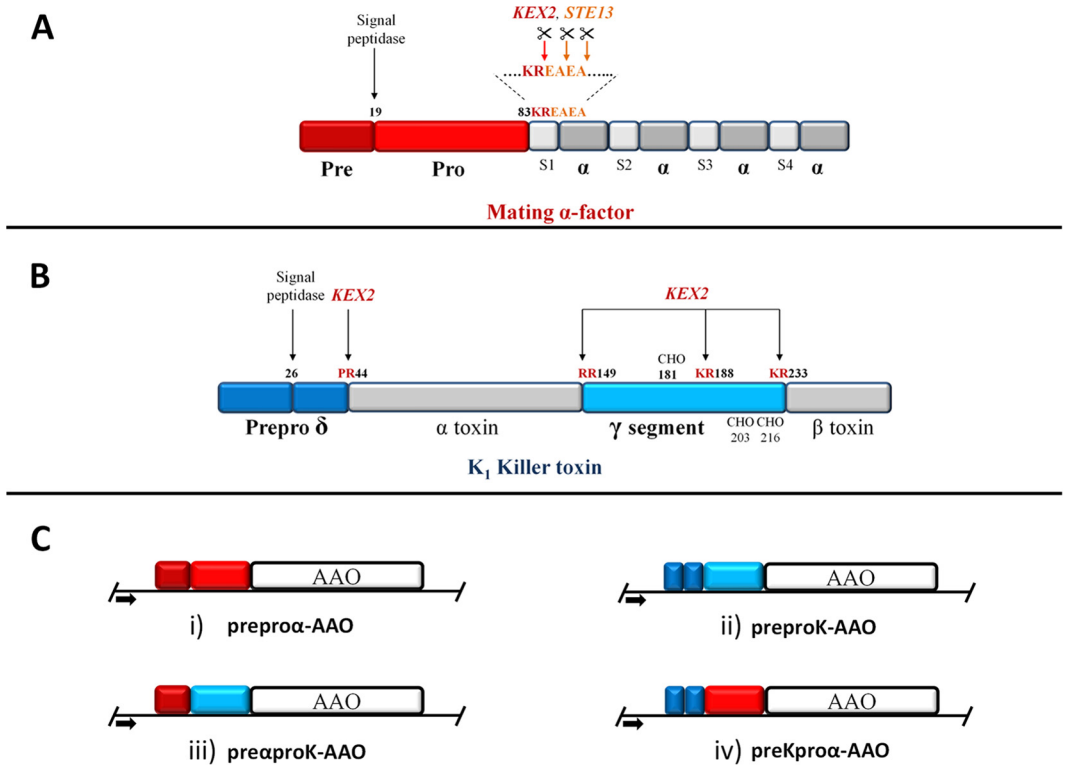

FIG 1 Prepro-leaders used and chimeric signal peptides engineered for functional AAO expression in *S. cerevisiae*. (A) Mating α-factor; (B) K1 killer preprotoxin; (C) AAO fusions for functional expression. The different processing sites for the KEX2 and STE13 signal peptidases are indicated in each case. The yeast mating pheromone α prepro-polyprotein precursor contains a hydrophobic N-terminal pre-sequence (dark red), followed by an N-glycosylated pro-sequence (red). The K1 killer toxin is derived from a 316 residue prepro-toxin. The unprocessed precursor consists of a prepro(δ) sequence (dark blue) that contains a 26-residue signal peptide. The γ segment (light blue) separating the alpha- and beta-toxin subunits was also used to engineer the chimeras.

were pooled, dialyzed against buffer P, concentrated, and loaded onto a high-resolution resin, strong-anion-exchange column (Biosuite MonoQ 10 cm; Waters, Milford, MA) preequilibrated in buffer P. The proteins were eluted with a linear gradient from 0 to 0.5 M NaCl in two phases at a flow rate of 1 ml/min: from 0 to 50% in 20 min and from 50 to 100% in 2 min. Fractions with AAO activity were pooled, dialyzed against buffer 20 mM phosphate buffer (pH 6.0), concentrated, and further purified by high-pressure liquid chromatography with a Superose 12 HR 10/30 molecular exclusion column (Amersham Bioscience) preequilibrated with 150 mM NaCl in phosphate buffer (pH 6.0) at a flow rate of 0.5 ml/min. The fractions with AAO activity were pooled, dialyzed against buffer (20 mM phosphate buffer [pH 6.0]), concentrated, and stored at −20°C. Throughout the purification protocol the fractions were analyzed by SDS-PAGE on 10% gels in which the proteins were stained with Protoblue Safe (National Diagnostics, USA). All protein concentrations were calculated using Bio-Rad protein assay reagent and bovine serum albumin (BSA) as the standard for the protein concentration.

(iii) Production and purification of native AAO from *E. coli*. Native heterologous AAO expressed in *E. coli* after *in vitro* refolding ($_{Ec}$AAO) was produced and purified as described elsewhere (17).

Biochemical characterization. (i) MALDI-TOF-MS analysis and pI determination. The matrix-assisted laser desorption ionization–time of flight mass spectrometry (MALDI-TOF-MS) experiments were performed on an Autoflex III MALDI-TOF-TOF instrument with a Smartbeam laser (Bruker Daltonics). The spectra were acquired using a laser power just above the ionization threshold, and the samples were analyzed in the positive-ion detection and delayed extraction linear mode. Typically, 1,000 laser shots were summed into a single mass spectrum. External calibration was performed using the BSA from Bruker, covering the range from 15,000 to 70,000 Da. Purified FX7 (8 μg) was subjected to two-dimensional electrophoresis gel in order to determine the pI.

(ii) N-terminal analysis. Purified AAO was subjected to SDS-PAGE, and the protein band was blotted onto polyvinylidene difluoride (PVDF) membranes. The PVDF membrane was stained with Coomassie brilliant blue R-250, and then the enzyme band was excised and processed for N-terminal amino acid sequencing on a precise sequencer at the core facilities of the Helmholtz Centre for Infection Research, Germany.

(iii) Determination of kinetic thermostability (T_{50}). Appropriate dilutions of purified FX7 and $_{Ec}$AAO were prepared for the assay, while the samples of parental preαproK-AAO were obtained from the crude supernatants. A temperature gradient scale ranging from 30 to 80°C was established as follows: 30.0, 31.4, 34.8, 39.3, 45.3, 49.9, 53, 55, 56.8, 59.9, 64.3, 70.3, 75, 78.1, and 80°C. This gradient profile was achieved using a thermocycler (Mycycler). After 10 min of incubation, FX7 and $_{Ec}$AAO samples were removed and chilled on ice for 10 min, followed by further incubation at room temperature for 5 min. Finally, 20-μl samples were added to 180-μl volumes of 100 mM sodium phosphate buffer (pH 6.0) containing 1 mM *p*-methoxybenzyl alcohol, and the activity was measured as anisaldehyde production by determining the absorption at 285 nm (ε_{285} = 16,950 M^{-1} cm^{-1}). In the case of parental preαproK-AAO supernatants, the samples were subjected to an HRP-ABTS assay described above for the screening. Thermostability values were calculated from the ratio between the residual activities incubated at different temperature points and the initial activity at room temperature. The T_{50} value was determined by the transition midpoint of the inactivation curve of the protein as a function of temperature, which in our case was defined as the temperature at which the enzyme lost 50% of its activity after an incubation of 10 min. All reactions were performed by triplicate.

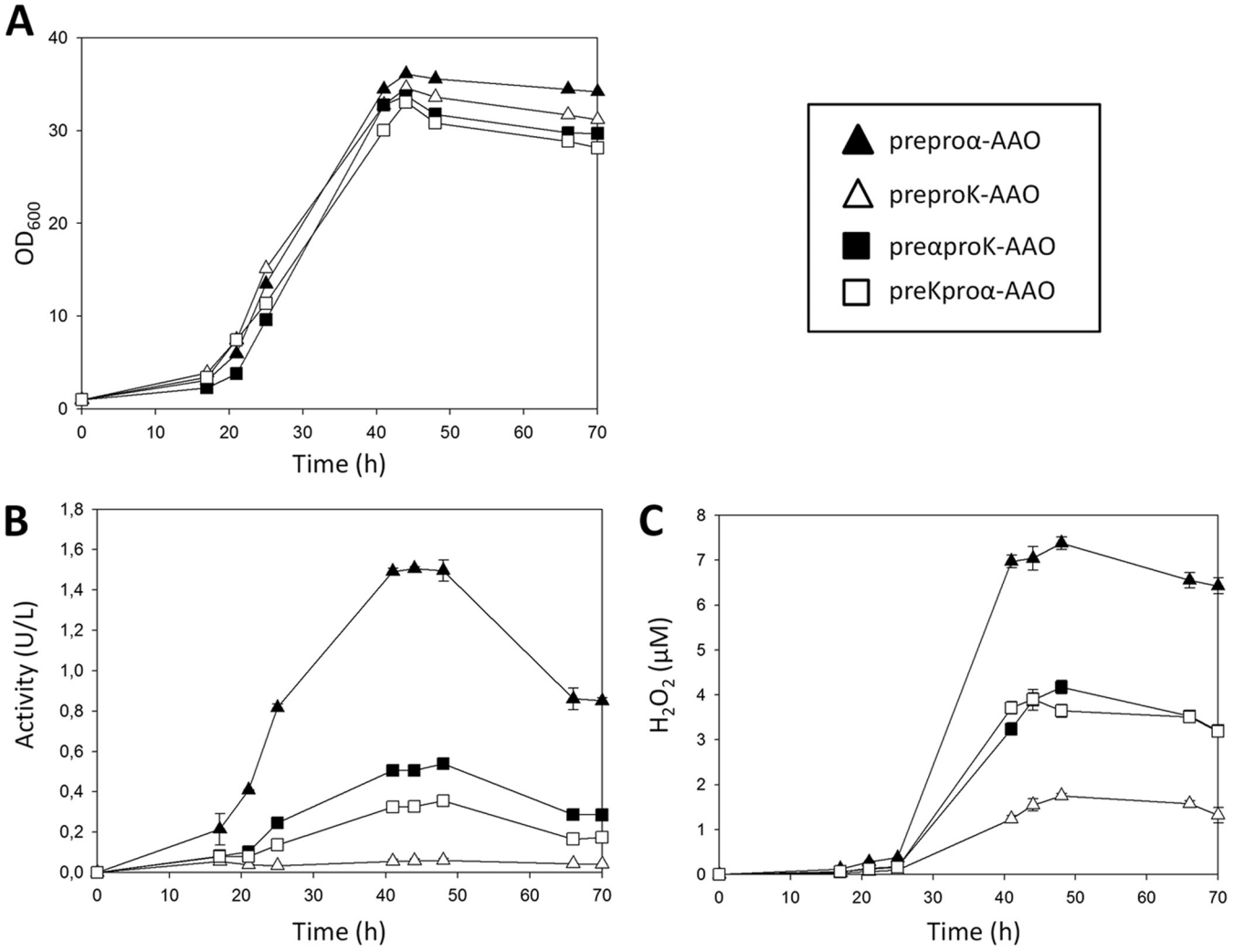

FIG 2 Expression of the AAO fusions in *S. cerevisiae*. (A) Shake flask fermentation growth curves; (B) AAO activity measured in an HRP-ABTS assay; (C) H_2O_2 production measured in a FOX assay. The preproα-AAO fusion achieved the highest yields in terms of cell growth and enzymatic activity (OD_{600} = 36; 1.5 U/liter after 44 h), followed by the preαproK-AAO, preKproα-AAO, and preproK-AAO fusions. Clone activity and H_2O_2 production were evaluated in triplicate, and each point includes the standard deviation.

(iv) Thermoactivity (T_a). Enzyme dilutions of purified FX7 (33 nM, final concentration) and $_{Ec}$AAO (18 nM, final concentration) were prepared in such a way that aliquots of 20 μl gave rise to a linear response in kinetic mode. The optimum temperature for activity was estimated in prewarmed 96-well reading plates (Labnet VorTemp 56 Shaking Incubator; Labnet International, USA) with 100 mM sodium phosphate (pH 6.0) containing 1 mM *p*-methoxybenzyl alcohol at various corresponding temperatures (25, 30, 40, 50, 60, 70, 80, 90, and 99°C), followed by incubation in an Eppendorf Thermomixer Comfort apparatus (Thermo Fisher Scientific). Reactions were performed by triplicate and *p*-methoxybenzyl alcohol oxidation, followed by aldehyde production at 285 nm.

(v) Kinetic parameters. Kinetic constants for AAO were estimated in 100 mM sodium phosphate (pH 6.0). The final enzyme concentrations used were as follows: with *p*-methoxybenzyl alcohol, 33 and 18 nM for FX7 and $_{Ec}$AAO, respectively; with veratryl alcohol, 38 and 32 nM for FX7 and $_{Ec}$AAO, respectively; with benzyl alcohol, 62 and 47 nM for FX7 and $_{Ec}$AAO, respectively; and with 2,4-hexadien-1-ol, 15 and 4 nM for FX7 and $_{Ec}$AAO, respectively. Reactions were performed in triplicate, and substrate oxidations were monitored by measuring the absorption at 285 nm for *p*-methoxybenzyl alcohol (ε_{285} = 16,950 M^{-1} cm^{-1}), 310 nm for veratryl alcohol (ε_{310} = 9,300 M^{-1} cm^{-1}), 250 nm for benzyl alcohol (ε_{250} = 13,800 M^{-1} cm^{-1}), and 280 nm for 2,4-hexadien-1-ol (ε_{280} = 30,140 M^{-1} cm^{-1}). Steady-state kinetic parameters were determined by fitting the initial reactions rates at different substrate concentrations to the Michaelis-Menten equation for one substrate, $v/e = k_{cat} \cdot S/(K_m + S)$, where e represents the enzyme concentration, k_{cat} is the maximal turnover rate, S is the substrate concentration, and K_m is the Michaelis constant. The data were fit using SigmaPlot 10.0 (Systat Software, Inc., Richmond, CA).

(vi) pH activity and stability profiles. Appropriate dilutions of enzyme samples were prepared in such a way that aliquots of 20 μl yielded a linear response in kinetic mode. The optimum pH activity was determined using 100 mM citrate-phosphate-borate buffer at different pH values (2.0, 3.0, 4.0, 5.0, 6.0, 7.0, 8.0, and 9.0) containing the corresponding alcohol concentration (0.3, 5, 9, and 1.2 mM for *p*-methoxybenzyl alcohol, veratryl alcohol, benzyl alcohol, and 2,4-hexadien-1-ol, respectively). To measure pH stability, enzyme samples were incubated at different times over a range of pH values. The residual activity was deduced from the activity before and after incubation with 0.3 mM *p*-methoxybenzyl alcohol in 100 mM phosphate buffer (pH 6.0).

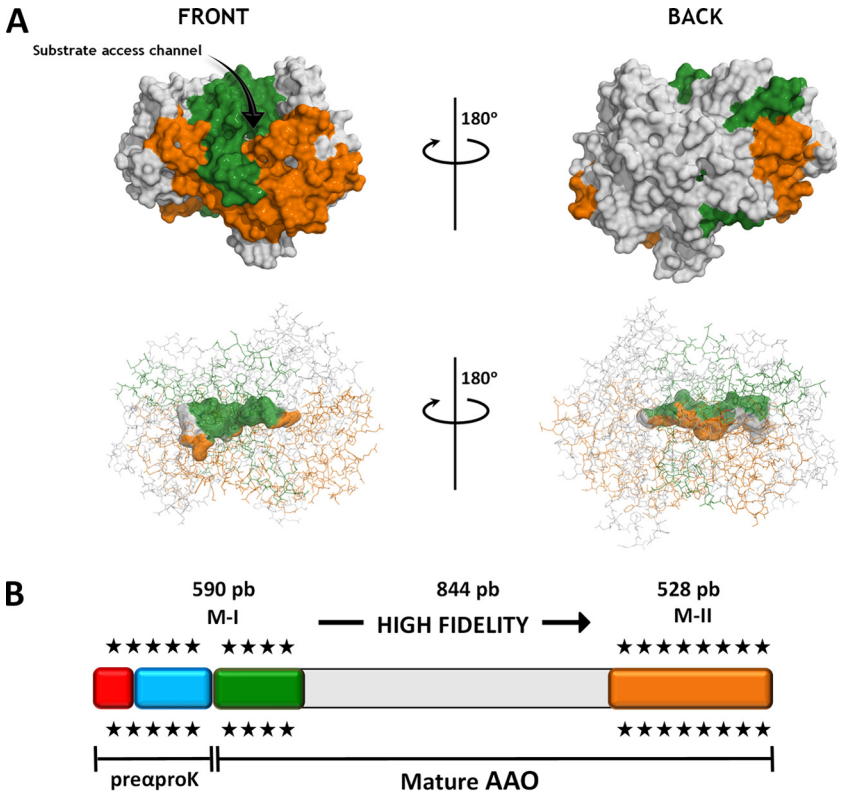

FIG 3 AAO segments for focused directed evolution. (A) The AAO structure is shown in front and back views as a surface mode (upper part), along with a detailed view of the FAD cavity (lower part). The mutagenic regions M-I and M-II are highlighted in green and orange, respectively. The gray region corresponds to the mutation-free segment. (B) The fusion gene preαproK-AAO is shown in color boxes (red and blue). Mutagenic region M-I contains preα (red box)-proK (blue box) signal peptide and the first 109 amino acid residues of mature AAO (green box). The mutagenic region M-II is shown as an orange box, and in gray is the region amplified with high-fidelity polymerase. Stars indicate the mutagenic regions in the fusion gene.

(vii) Protein modeling. The crystal structure of the AAO from *P. eryngii* at a resolution of 2.55 Å (Protein Data Bank Europe [PDB] accession number 3FIM [31]) was used for the FX7 mutant homology model, obtained by PyMol (Schrodinger, LLC [http://www.pymol.org]).

(viii) DNA sequencing. All genes were verified by DNA sequencing (using a BigDye Terminator v3.1 cycle sequencing kit). The primers used were common to the four constructions: sense primers RMLN and AAOsec1F (5′-GTGGATCAACAGAAGATTTCGATCG-3′) and antisense primers RMLC (5′-GCTTACATTCACGCCCTCCC-3′), AAOsec2R (5′-GTGGTTAGCAATGAGCGCGG-3′), and AAOsec3R (5′-GGAGTCGAGCCTCTGCCCCT-3′).

RESULTS AND DISCUSSION

Construction of chimeric signal prepro-leaders. In terms of yeast expression, the replacement of native signal peptides to foster foreign protein secretion has been used widely for years. Recently, the directed evolution of the α-factor prepro-leader permitted the functional expression of antibodies (32) and different classes of ligninases (including high-redox potential laccases, versatile peroxidases, and unspecific peroxygenases) (18–22). In the present study, the prepro-leaders from the mating α-factor and the K_1 killer toxin, along with their chimeric combinations, were tailored and attached to the native AAO for functional expression and directed evolution. The mating α-factor signal sequence is formed by 19 and 64 amino acids from the pre- and pro-leaders, respectively (33–35) (Fig. 1A). The pre-leader initiates endoplasmic reticulum translocation, and it is finally removed by the action of a signal peptidase that cuts between residues 19 and 20. The pro-leader contains three Asn-linked glycosylation sites, and it is thought to be involved in the folding and maturation of the protein before it is packed into vesicles for exocytosis. The pro-leader is processed in the Golgi compartment by the action of the KEX2, STE13, and KEX1 proteases, although the latter is not needed for heterologous protein secretion. The K_1 killer prepro-toxin is preceded by a prepro-sequence of 44 residues, prepro(δ), that undergoes similar processing as the α-factor prepro-leader, albeit without the requirement of STE13 and KEX1 activity (24, 25, 36) (Fig. 1B). The prepro-toxin contains an internal γ-segment of 85 residues with three extra KEX2 recognition sites for processing in the Golgi compartment. Bearing in mind the common features of these two prepro-leaders in terms of processing and secretion, the following four fusion constructs were attached to the mature AAO (Fig. 1C): (i) the preproα-AAO containing the full α-factor prepro-leader, (ii) the preproK-AAO formed by the prepro(δ) of K_1 toxin connected to a truncated version (64 residues) of the γ-segment known to be important for correct processing (the truncated segment stretched from positions 169 to 233 and preserved the three N-glycosylation sites: N181, N203, and N216 [24]), (iii) the chimeric preαproK-AAO comprising the α-factor pre-leader fused to the truncated γ-segment, and (iv) the chimeric preKproα-AAO formed by the prepro(δ) of the K_1 toxin linked to the α-factor pro-leader. In addition, we modified the prepro(δ)-containing constructs, fusions ii and iv, by site-directed mutagen-

TABLE 1 Selected mutants of preαproK-AAO libraries

Variant	Library	Mutation	Location	Secondary motif	Total activity improvement (fold)[a]	T_{50} (°C)
FX7	M-I-II	$_{CAC}$H91N$_{AAC}$	FAD-binding domain	Loop	96	64.3
13H2	M-IV	$_{ATA}$I194V$_{GTA}$	Substrate-binding domain	Loop	4.9	60.8
10G5	M-IV	$_{TTG}$L170 M$_{ATG}$	Substrate-binding domain	Alpha helix	4.9	60.5
7A11	M-II	$_{GAT}$D341N$_{AAT}$	Substrate-binding domain	Alpha helix	4.6	59.3
4C7	M-II	$_{AGA}$R481S$_{AGT}$	Substrate-binding domain	Loop	4.5	61.5
12G12	M-I	$_{ACA}$T[50K]A$_{GCA\ AGC}$S88T$_{ACC}$	Signal peptide; FAD-binding domain	Loop	1.9	61.8
PreαproK-AAO (parental type)					1	58.8
$_{Ec}$AAO						47.5

[a] The total activity improvement over parental type was estimated with 2 mM *p*-methoxybenzylalcohol as the substrate in 100 mM phosphate buffer (pH 6.0).

esis to modify the P43-R44 KEX2 recognition site to K43-R44, since this substitution was associated with a 50-fold enhancement in KEX2 catalytic efficiency (37).

The fusion constructs were spliced in *S. cerevisiae*, and taking advantage of the high frequency of *in vivo* homologous DNA recombination of this yeast overlapping areas of ~50 bp guaranteed correct DNA assembly of the different genetic elements and the linearized plasmid without altering the open reading frame (38). The activity of each AAO construct against veratryl alcohol was assayed in microscale fermentations (96-well plates), and the four fusions produced detectable AAO activity in the culture broth, which was consistent in the two colorimetric assays used (see below). The secretion driven by the corresponding constructs was as follows: preproα-AAO > preαproK-AAO > preKproα-AAO > preproK-AAO. We verified by DNA sequencing that the constructs did not incorporate mutations in the mature protein or in the prepro-sequences (apart from the aforementioned P43K substitution) and that all of the elements were properly assembled *in vivo* as intended. Fermentations were translated from the high-throughput format to larger volumes (10 ml) for each construct studied. Irrespective of the substrate (*p*-methoxybenzyl or veratryl alcohol), the hierarchy of activity of the fusion genes was maintained: preproα-AAO (1.5 U/liter), preαproK-AAO (0.5 U/liter), preKproα-AAO (0.35 U/liter), and preproK-AAO (0.06 U/liter) (Fig. 2). We tried to enhance the membrane permeability of the yeast by adding ethanol to the expression medium, and yet the activity detected was 5-fold lower, which was probably due to growth inhibition as a consequence of changes in yeast physiology and the redox balance of the medium (39).

TABLE 2 Biochemical properties of recombinant native $_{Ec}$AAO and evolved AAO (FX7 mutant)

Biochemical properties	$_{Ec}$AAO	FX7 mutant
Molecular mass (Da)[a]		
SDS-PAGE	65,000	120,000
MALDI-TOF-MS	61,847[c]	61,485
Amino acid composition	61,088	60,934
Glycosylation degree (%)		50
Thermal stability (T_{50} [°C])	47.5	64.3
pI	3.9	4.3
N-terminal end sequence	MADFDYVVG[d]	ADFDYVVVG
Sp act (U/mg)[b]	74	24
Secretion level (mg/liter)		2

[a] Masses were estimated based on SDS-PAGE, MALDI-TOF-MS after deglycosylation with PNGase F, or the amino acid composition.
[b] That is, the specific activity for *p*-methoxybenzyl alcohol.
[c] This information was obtained from reference 17.
[d] Met1 (M) was added to the N-terminal end for cloning in *E. coli*.

Directed evolution of preαproK-AAO. Of the four AAO constructs, the preproα-AAO produced the highest secretion, although the risk of inefficient processing of the α-pro-leader by STE13 ruled out its use. Given that little STE13 is found in the Golgi apparatus, the secreted heterologous protein maintains an extra EAEA spacer dipeptide at the N terminus, as previously demonstrated in the evolution of other oxidoreductases fused to preproα (laccases and peroxidases) (18, 20, 40). This problem may be circumvented by (i) suppressing the cleavage site for STE13, (ii) enhancing the expression of STE13, or (iii) deleting the whole α-factor pro-leader. However, this may drive the intracellular accumulation and/or the secretion of partially processed forms, no matter the strategy used (41). It is worth noting that the N-terminal of AAO interacts with the FAD molecule through a network of H bonds, such that an extra-N-terminal sequence could modify these contacts, jeopardizing catalysis (30, 42). Since a correct processing is crucial to conserve the integrity and orientation of the attached FAD cofactor in the tertiary structure of AAO, the preαproK-AAO construct, in which the proK fragment is exclusively processed by the abundant KEX2, was chosen as the point of departure for engineering.

To enhance the activity and secretion of the preαproK-AAO in yeast several mutant libraries were constructed by conventional and guided-directed evolution. The latter was performed by MORPHING, a one-pot focused domain mutagenesis method supported by the *in vivo* gap repair mechanism of *S. cerevisiae* (26). By MORPHING, we can direct random mutations and recombination events to short sequences, while keeping the remaining parts of the gene unaltered. Two protein segments of the preαproK-AAO (M-I, Met[α1]-Val109; M-II, Phe392-Gln566) were studied simultaneously through this approach (Fig. 3). The M-I segment includes the preαproK (to evolve the chimeric leader for secretion) plus a region of the mature AAO (Ala1-Val109) that contains the FAD-binding domain at its N terminus, along with several structural determinants in the nearby substrate access channel: Val54, Pro55, His91, Tyr92, Pro79, and Val90 (4, 6, 30). The M-II segment contains the catalytic pocket, including the His546 involved in substrate positioning, the catalytic base His502, and the aromatic residues Phe397 and Phe501. These latter amino acids create a hydrophobic gate in conjunction with Tyr92 of the M-I segment, thereby blocking access to the active channel (1, 4, 30). A total of three focused mutant libraries were

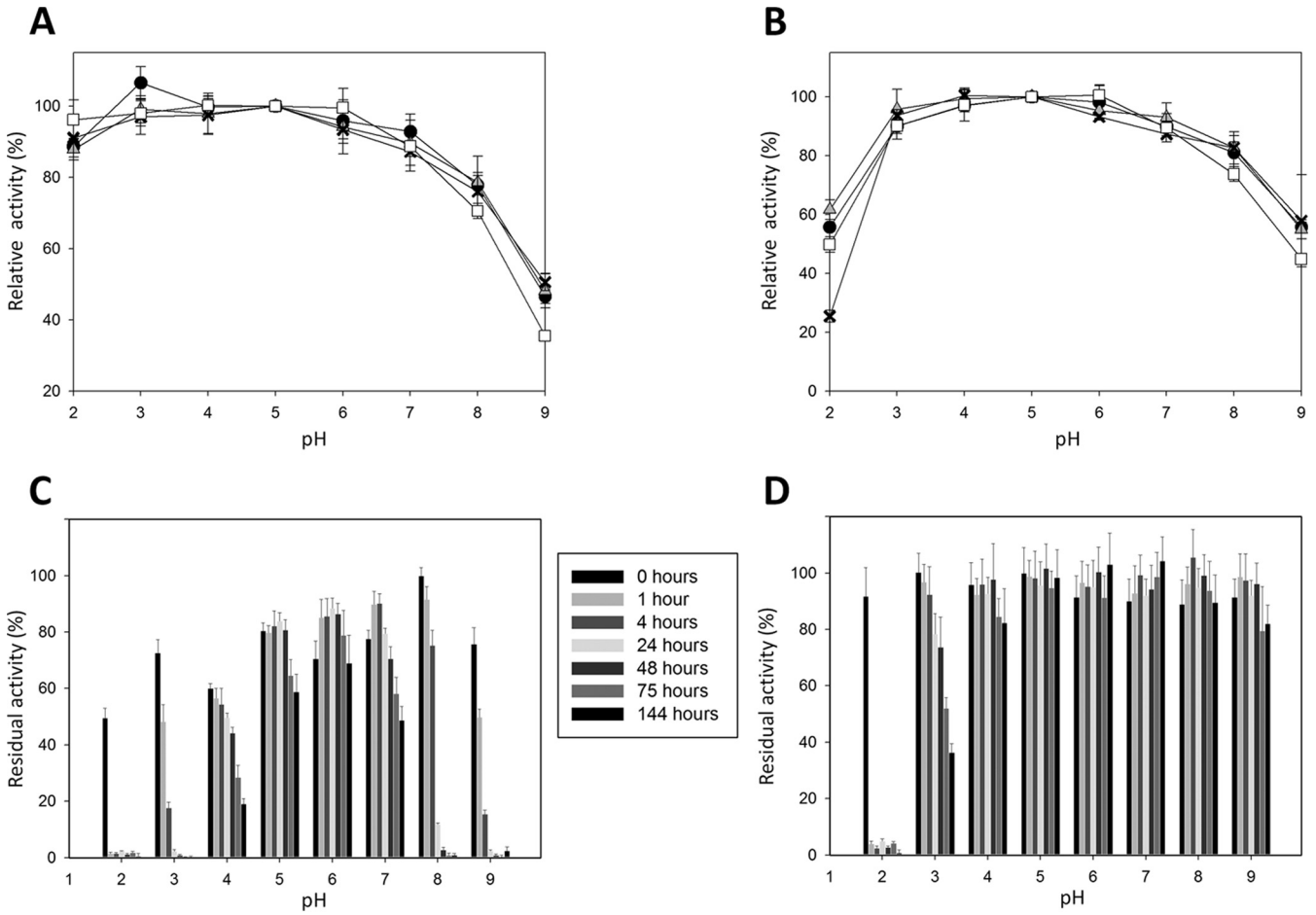

FIG 4 pH activity and stability. (A and B) pH activity profiles for $_{Ec}$AAO (A) and FX7 (B). Activities were measured in 100 mM citrate-phosphate-borate buffer at different pH values. Symbols: black circles, *p*-methoxybenzyl alcohol; gray triangles, veratryl alcohol; crosses, benzyl alcohol; white squares, 2,4-hexadien-1-ol. (C and D) pH stability of $_{Ec}$AAO (C) and FX7 (D). Enzymes samples were incubated in 100 mM citrate-phosphate-borate buffer at different pH values, and the residual activity was measured with 0.3 mM *p*-methoxybenzyl alcohol in 100 mM phosphate buffer (pH 6.0). The results represent the means and standard deviations of three independent experiments.

constructed (single M-I and M-II, as well as M-I-II combined), in addition to one conventional mutant library (targeting the full preαproK-AAO by random mutation and DNA recombination; M-IV). Mutational loads were adjusted to introduce 1 to 3 amino acid changes per protein, and the four libraries were explored with a highly sensitive dual HTS system to detect AAO activity irrespective of the substrate. This method coupled a standard HRP-ABTS indirect colorimetric assay to a direct chemical method (FOX) based on the Fenton reaction in order to detect H_2O_2. The latter is typically used to measure H_2O_2 in biological fluids, and more recently to determine L-amino acid oxidase and lipoxygenase activities (27, 28, 43, 44), but to our best knowledge it has never been used to evolve H_2O_2-producing enzymes. The limit of sensitivity of the FOX assay was 2 μM H_2O_2, and it was further shifted to 0.4 μM H_2O_2 through the inclusion of sorbitol to propagate the response (see Materials and Methods for details). Two consecutive rescreenings were carried out to avoid the selection of false positives. After exploring ~5,000 clones, we identified five mutants with a total activity improvement over the parental type ranging from 2- to 5-fold and, significantly, the FX7 variant (H91N) from the combined M-I-II MORPHING displayed a dramatic 96-fold improvement in total activity with respect to the parental type (Table 1). The remaining mutations found in these variants (i.e., T[$K_1$50]A, S88T, L170M, I194V, D341N, and R481S) are located at a distance of >20 residues from one another, making them suitable candidates for future DNA shuffling studies or to be evaluated by site-directed recombination (see Fig. S1 in the supplemental material).

Biochemical characterization. The FX7 variant was purified to homogeneity and characterized biochemically. Since the weak secretion of parental preαproK-AAO (0.5 U/liter) in *S. cerevisiae* hindered its purification, the properties of purified FX7 were compared to that of the native AAO heterologous expressed in *E. coli* after *in vitro* refolding ($_{Ec}$AAO). FX7 was secreted at 2 mg/liter with a specific activity for *p*-methoxybenzyl alcohol of 24 U/mg (Table 2). Both FX7 and $_{Ec}$AAO enzymes showed similar kinetic constants, as well as pH activity profiles, with all of the substrates tested (Fig. 4A and B), although turnover rates (k_{cat}) were lower if the enzyme is expressed in *S. cerevisiae* instead of *E. coli* (Table 3). The N-terminal sequencing of FX7 confirmed the correct cleavage of the chimeric preαproK-leader, avoiding unwanted modifications at the N terminus. FX7 was heavily glycosylated (~50% gly-

TABLE 3 Kineticparameters of native $_{Ec}$AAO and evolved AAO (FX7 mutant)[a]

Substrate	Kinetic constant	$_{Ec}$AAO		FX7	
		Mean	SEM	Mean	SEM
p-Methoxybenzyl alcohol	K_m (mM)	0.035	0.001	0.034	0.001
	k_{cat} (s^{-1})	105	6	54	4
	k_{cat}/K_m (s^{-1} mM^{-1})	2979	66	1562	44
Veratryl alcohol	K_m (mM)	0.504	0.043	0.388	0.023
	k_{cat} (s^{-1})	66	2	28	1
	k_{cat}/K_m (s^{-1} mM^{-1})	131	8	71	3
Benzyl alcohol	K_m (mM)	0.770	0.011	0.510	0.001
	k_{cat} (s^{-1})	22	1	19	1
	k_{cat}/K_m (s^{-1} mM^{-1})	28	2	36	3
2,4-Hexadien-1-ol	K_m (mM)	0.087	0.001	0.059	0.004
	k_{cat} (s^{-1})	136	3	52	1
	k_{cat}/K_m (s^{-1} mM^{-1})	1555	67	866	53

[a] Steady-state constants were estimated in 100 mM sodiumphosphate buffer (pH 6) at 24°C. All reactions were performed intriplicate.

cosylation), adopting a molecular mass of ~120,000 Da, and yet after deglycosylation the AAO smear collapsed to a single band of around 61,000 Da, as confirmed by MALDI-TOF analysis (Table 2 and see Fig. S2 in the supplemental material). It is well known that *S. cerevisiae* tends to hyperglycosylate heterologous proteins; possibly, a slow transit of AAO through the Golgi compartment before its packing into vesicles for exocytosis facilitates the addition of long chains of mannose moieties that can cover the protein surface as reported for many other hyperglycosylated enzymes in *S. cerevisiae* (34). The use of glycosylation-deficient *S. cerevisiae* strains (e.g., a Δ*kre2* mutant that is only capable of attaching smaller mannose oligomers [45]) could have lightened the strong AAO glycosylation, albeit at the possible cost of endangering secretion, given that the *S. cerevisiae* strain used in our study is protease deficient. Hyperglycosylation can exert a beneficial stability effect. Indeed, the T_{50} (the temperature at which the enzyme retains 50% of its initial activity after a 10-min incubation) was ~11°C above that of $_{Ec}$AAO for all of the AAO variants expressed in *S. cerevisiae*, with a further 5.5°C increase for FX7 that must be exclusively attributed to beneficial H91N mutation (from 47.5 to 64.3°C) (Table 1 and Fig. 5A). This high thermostability correlated with a stronger thermoactivity (i.e., the optimum temperature for activity [T_a]). Thus, the T_a of FX7 was over 80% at 80°C, whereas $_{Ec}$AAO conserved 22% activity at the same temperature (Fig. 5B). Notably, FX7 still maintained ~60 and 20% activities at 90 and 100°C, respectively, whereas the $_{Ec}$AAO T_a was negligible. Moreover, FX7 showed a broad pH stability in the range of 3 to 9 (Fig. 4C and D). After 144 h of incubation, the residual FX7 activities were ~80 and 38% at pH 3 and 9, respectively, whereas the residual $_{Ec}$AAO activities at those pH values were negligible.

It is worth noting that His91 is a deviation in *P. eryngii* and *P. pulmonarius* AAO, since an Asn lies at this position in virtually all members of the GMC superfamily, including 70 putative AAO sequences from different basidiomycetes (10) (Fig. 6A). Hence, restoring this consensus mutation has been crucial to improve heterologous AAO expression in yeast while enhancing thermostability, which is in excellent agreement with previous reports on ancestral library design by introducing consensus/ancestor mutations to improve the heterologous expression and thermostability of different enzymes (46–48). Indeed, the discovery of a consensus mutation by focused evolution, rather than using the consensus method based on sequence alignment or an inference phylogenetic analysis for ancestor mutations, highlights the potential of random domain mutagenesis approaches to reveal beneficial consensus/ancestor mutations. H91N lies in the flavin attachment loop region, a common motif in GMC oxidoreductases. Found on the *si*-face of the isoalloxazine ring, hydrophobic interactions of this residue maintain the cofactor in a bent conformation (49). In *P. eryngii* AAO, His91 interacts with Arg206 (Arg/Lys of other GMC proteins), and it stabilizes the flavin ring conformation (Fig. 6). The substitution of a positively charged His by a polar uncharged Asn may alter these contacts in *P. eryingii* AAO, which could aid the attachment of FAD and enhance the stability and functional expression. The two latter properties are strongly connected, and it is highly likely that the improved stability allows more AAO to be secreted, as it has been described for many other proteins expressed in yeast (50). Why the N91H substitution arose exclusively in the natural evolution of *P. eryngii* and *P. pulmonarius* AAO is unclear, and yet our results suggest a possible reg-

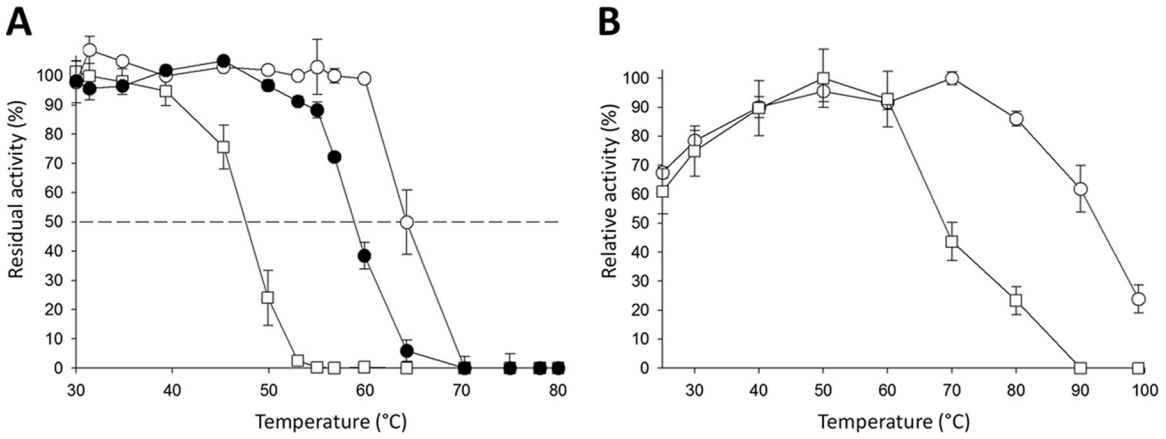

FIG 5 Thermostability and thermoactivity of AAO variants. (A) Thermostability (T_{50}) of FX7 (○), preαproK-AAO parental type (●), and $_{Ec}$AAO (□). (B) Thermoactivity (T_a) of FX7 (○), and $_{Ec}$AAO (□). Each point represents the means and standard deviations of three independent experiments.

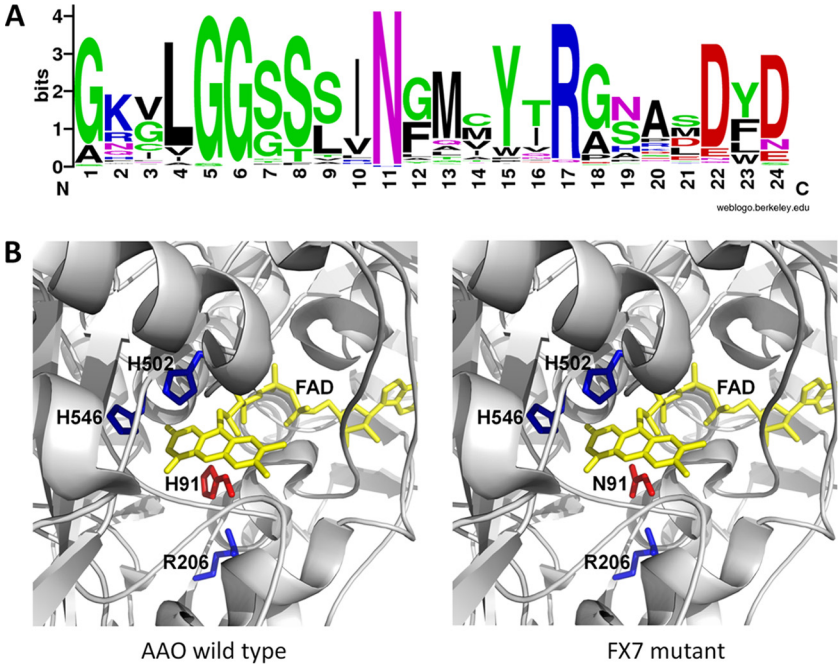

FIG 6 (A) Consensus Asn91 in GMC superfamily. Sequence logo of the GMC signature 1 (prosite PS00623) in 329 GMC sequences from GenBank (http://www.ncbi.nlm.nih.gov/GenBank/), JGI (http://jgi.doe.gov/), and Prosite Expasy (http://prosite.expasy.org/PS00623), including cholesterol oxidase, choline oxidase, aryl-alcohol oxidase, pyridoxine oxidase, methanol oxidase, glucose oxidase and dehydrogenase, pyranose oxidase and dehydrogenase, cellobiose dehydrogenase, L-sorbose-1-dehydrogenase, and hydroxynitrile lyase proteins. (B) N91H mutation in FX7 variant. A molecular model using as the template the *P. eryngii* AAO crystal structure (PDB code 3FIM) was prepared to map the mutation. The residues of the active site His502, His546, and R206 are depicted in blue, FAD is depicted in yellow, and the H91N mutation is depicted in red.

ulation of AAO expression to reduce the inhibition of ligninolytic peroxidases by H_2O_2 (51).

Conclusions and outlook. In this study, the AAO from *P. eryngii* was functionally expressed in *S. cerevisiae* by engineering chimeric prepro-leaders that allowed us to construct and screen mutant libraries in yeast. The particular design of an *ad hoc* chimeric prepro-leader, combined with a focused-directed evolution strategy and a sensitive dual screening assay, has led to obtain an active, highly stable AAO variant that is secreted by yeast as a correctly processed enzyme.

Although hardly used, the biotechnological potential of AAO should not be underestimated. In nature, the gradual release of H_2O_2 by AAO supplies peroxidases with a continuous source of cooxidant for lignin degradation. *In vitro*, this effect can be mimicked by controlling the addition of H_2O_2 with sensors and peristaltic pumps, although with limited success (52). Very recently, we introduced the FX7 variant into episomal bidirectional vectors to coexpress versatile peroxidase-AAO and/or unspecific peroxygenase-AAO (unpublished data). These self-sufficient expression systems could be used to evolve efficient enzymatic cascade reactions (e.g., for the oxidative conversion of 5-hydroxymethylfurfurals into value-added chemicals [53]). Significantly, the FX7 variant and its future offspring could also be included to design an autonomously consolidated bioprocessing yeast, with a full artificial secretome that includes the most important elements of the ligninolytic enzyme consortium. Such a microbe would have a number of potential applications in lignocellulose biorefineries for the production of fuels and commodities (22, 54). Finally, the directed evolution platform presented here is an invaluable tool for protein engineering, which can be applied from the design of efficient stereoselective aryl secondary alcohol oxidases to the synthesis of natural flavors (1).

ACKNOWLEDGMENTS

This study was supported by the European Commission projects Indox-FP7-KBBE-2013-7-613549 and Cost-Action CM1303-Systems Biocatalysis and by the National Projects Dewry (BIO201343407-R) and Cambios (RTC-2014-1777-3).

REFERENCES

1. **Hernandez-Ortega A, Ferreira P, Martinez AT.** 2012. Fungal aryl-alcohol oxidase: a peroxide-producing flavoenzyme involved in lignin degradation. Appl Microbiol Biotechnol **93:**1395–1410. http://dx.doi.org/10.1007/s00253-011-3836-8.
2. **Ruiz-Dueñas FJ, Martinez AT.** 2009. Microbial degradation of lignin: how a bulky recalcitrant polymer is efficiently recycled in nature and how we can take advantage of this. Microb Biotechnol **2:**164–177. http://dx.doi.org/10.1111/j.1751-7915.2008.00078.x.
3. **Ferreira P, Hernandez-Ortega A, Herguedas B, Rencoret J, Gutierrez A, Martinez MJ, Jimenez-Barbero J, Medina M, Martinez AT.** 2010. Kinetic and chemical characterization of aldehyde oxidation by fungal aryl-alcohol oxidase. Biochem J **425:**585–593. http://dx.doi.org/10.1042/BJ20091499.
4. **Ferreira P, Ruiz-Dueñas FJ, Martinez MJ, van Berkel WJH, Martinez AT.** 2006. Site-directed mutagenesis of selected residues at the active site of aryl-alcohol oxidase, an H_2O_2-producing enzyme. FEBS J **273:**4878–4888. http://dx.doi.org/10.1111/j.1742-4658.2006.05488.x.
5. **Ferreira P, Hernandez-Ortega A, Herguendas B, Martinez AT, Medina M.** 2009. Aryl-alcohol oxidase involved in lignin degradation: a mechanistic study based on steady and pre-steady-state kinetics and primary and solvent isotope effects with two different alcohol substrates. J Biol Chem **284:**24840–24847. http://dx.doi.org/10.1074/jbc.M109.011593.
6. **Hernandez-Ortega A, Lucas F, Ferreira P, Medina M, Guallar V, Martinez AT.** 2011. Modulating O_2 reactivity in a fungal flavoenzyme: in-

volvement of aryl-alcohol oxidase Phe-501 contiguous to catalytic histidine. J Biol Chem **286:**41105–41114. http://dx.doi.org/10.1074/jbc.M111.282467.
7. **Hernandez-Ortenga A, Borreli K, Ferreira P, Medina M, Martinez AT, Guallar V.** 2011. Substrate diffusion and oxidation in GMC oxidoreductases: an experimental and computational study on fungal aryl-alcohol oxidase. Biochem J **436:**341–350. http://dx.doi.org/10.1042/BJ20102090.
8. **Hernandez-Ortega A, Ferreira P, Merino P, Medina M, Guallar V, Martinez AT.** 2012. Stereoselective hydride transfer by aryl-alcohol oxidase, a member of the GMC superfamily. Chembiochem **13:**427–435. http://dx.doi.org/10.1002/cbic.201100709.
9. **Hernandez-Ortega A, Lucas F, Ferreira P, Medina M, Guallar V, Martinez AT.** 2012. Role of active site histidines in the two half reactions of the aryl-alcohol oxidase catalytic cycle. Biochemistry **51:**6595–6608. http://dx.doi.org/10.1021/bi300505z.
10. **Ferreira P, Hernandez-Ortega A, Lucas F, Carro J, Herguedas B, Borreli KW, Guallar V, Martinez AT, Milagros M.** 2015. Aromatic stacking interactions govern catalysis in aryl-alcohol oxidase. FEBS J http://dx.doi.org/10.1111/febs.13221.
11. **Bloom JD, Arnold FH.** 2009. In the light of directed evolution: pathways of adaptive protein evolution. Proc Natl Acad Sci U S A **106:**9995–10000. http://dx.doi.org/10.1073/pnas.0901522106.
12. **Turner NJ.** 2009. Directed evolution drives the next generation of biocatalysts. Nat Chem Biol **5:**567–573. http://dx.doi.org/10.1038/nchembio.203.
13. **Jackel C, Hilvert D.** 2010. Biocatalysts by evolution. Curr Opin Biotechnol **21:**753–759. http://dx.doi.org/10.1016/j.copbio.2010.08.008.
14. **Bornscheuer UT, Huisman GW, Kazlauskas RJ, Lutz S, Moore JC, Robins K.** 2012. Engineering the third wave of biocatalysis. Nature **485:**185–194. http://dx.doi.org/10.1038/nature11117.
15. **Varela E, Guillen F, Martinez AT, Martinez MJ.** 2001. Expression of *Pleurotus eryngii* aryl-alcohol oxidase in *Aspergillus nidulans*: purification and characterization of the recombinant enzyme. Biochim Biophys Acta **1546:**107–113. http://dx.doi.org/10.1016/S0167-4838(00)00301-0.
16. **Pourmir A, Johannes TW.** 2012. Directed evolution selection of the host organism. Comp Struct Biotechnol J **2:**e201209012. http://dx.doi.org/10.5936/csbj.201209012.
17. **Ruiz Dueñas FJ, Ferreira P, Martínez MJ, Martínez AT.** 2006. *In vitro* activation, purification, and characterization of *Escherichia coli* expressed aryl-alcohol oxidase, a unique H_2O_2-producing enzyme. Prot Expr Purif **45:**191–199. http://dx.doi.org/10.1016/j.pep.2005.06.003.
18. **Mate D, Garcia-Burgos C, Garcia-Ruiz E, Ballesteros AO, Camarero S, Alcalde M.** 2010. Laboratory evolution of high redox potential laccases. Chem Biol **17:**1030–1041. http://dx.doi.org/10.1016/j.chembiol.2010.07.010.
19. **Camarero S, Pardo I, Cañas AI, Molina P, Record E, Martinez AT, Martinez MJ, Alcalde M.** 2012. Engineering platforms for directed evolution of laccase from *Pycnoporus cinnabarinus*. Appl Environ Microbiol **78:**1370–1384. http://dx.doi.org/10.1128/AEM.07530-11.
20. **Garcia-Ruiz E, Gonzalez-Perez D, Ruiz-Dueñas FJ, Martinez AT, Alcalde M.** 2012. Directed evolution of a temperature, peroxide and alkaline pH tolerant versatile peroxidase. Biochem J **441:**487–498. http://dx.doi.org/10.1042/BJ20111199.
21. **Molina-Espeja P, Garcia-Ruiz E, Gonzalez-Perez D, Ullrich R, Hofrichter M, Alcalde M.** 2014. Directed evolution of unspecific peroxygenase from *Agrocybe aegerita*. Appl Environ Microbiol **80:**3496–3507. http://dx.doi.org/10.1128/AEM.00490-14.
22. **Alcalde M.** 2015. Engineering the ligninolytic enzyme consortium. Trends Biotechnol **33:**155–162. http://dx.doi.org/10.1016/j.tibtech.2014.12.007.
23. **Garcia-Ruiz E, Mate DM, Gonzalez-Perez D, Molina-Espeja P, Camarero S, Martinez AT, Ballesteros AO, Alcalde M.** 2014 Directed evolution of ligninolytic oxidoreductases: from functional expression to stabilization and beyond, p 1–18. *In* Fessner R (ed), Cascade biocatalysis. Wiley-VCH, Weinheim, Germany.
24. **Cartwright C, Zhu Y, Tipper DJ.** 1992. Efficient secretion in yeast based on fragments from K1 killer preprotoxin. Yeast **8:**261–272. http://dx.doi.org/10.1002/yea.320080404.
25. **Zhu Y, Kane J, Zhang X, Zhang M, Tipper DJ.** 1993. Role of the γ component of the preprotoxin in expression of the yeast K1 killer phenotype. Yeast **9:**251–266. http://dx.doi.org/10.1002/yea.320090305.
26. **Gonzalez-Perez D, Molina-Espeja P, Garcia-Ruiz E, Alcalde M.** 2014. Mutagenic organized recombination process by homologous in vivo grouping (MORPHING) for directed enzyme evolution. PLoS One **9:**e90919. http://dx.doi.org/10.1371/journal.pone.0090919.
27. **Gay C, Collins J, Gebicki JM.** 1999. Hydroperoxide assay with the ferric-xylenol orange complex. Anal Biochem **273:**149–155. http://dx.doi.org/10.1006/abio.1999.4208.
28. **Rhee SG, Chang T, Jeong W, Kang D.** 2010. Methods for detection and measurement of hydrogen peroxide inside and outside of cells. Mol Cells **29:**539–549. http://dx.doi.org/10.1007/s10059-010-0082-3.
29. **Bou R, Codony R, Tres A, Decker EA.** 2008. Determination of hydroperoxides in foods and biological samples by the ferrous oxidation-xylenol orange method: a review of the factors that influence the method's performance. Anal Biochem **337:**1–15.
30. **Shrivastava A, Gupta VB.** 2011. Methods for the determination of limit of detection and limit of quantitation of the analytical methods. Chron Young Sci **2:**21–25. http://dx.doi.org/10.4103/2229-5186.79345.
31. **Fernandez IS, Ruiz-Dueñas FJ, Santillana E, Ferreira P, Martinez MJ, Martinez AT, Romero A.** 2009. Novel structural features in the GMC family of oxidoreductases revealed by the crystal structure of fungal aryl-alcohol oxidase. Acta Crystallogr D Biol Crystallogr **65:**1196–1205. http://dx.doi.org/10.1107/S0907444909035860.
32. **Rakestraw JA, Sazinsky SL, Piatesi A, Antipov E, Wittrup KD.** 2009. Directed evolution of a secretory leader for the improved expression of heterologous proteins and full-length antibodies in *Saccharomyces cerevisiae*. Biotechnol Bioeng **103:**1192–1201. http://dx.doi.org/10.1002/bit.22338.
33. **Zsebo KM, Lu HS, Fieschko JC, Goldstein L, Davis J, Duker K, Suggs SV, Lai PH, Bitter GA.** 1986. Protein secretion from *Saccharomyces cerevisiae* directed by the prepro-α-factor leader region. J Biol Chem **261:**5858–5865.
34. **Shuster JR.** 1991. Gene expression in yeast: protein secretion. Curr Opin Biotechnol **2:**685–690. http://dx.doi.org/10.1016/0958-1669(91)90035-4.
35. **Romanos MA, Scorer CA, Clare JJ.** 1992. Foreign gene expression in yeast: a review. Yeast **8:**423–488. http://dx.doi.org/10.1002/yea.320080602.
36. **Schmitt MJ, Breinig F.** 2006. Yeast viral killer toxins: lethality and self-protection. Nat Rev Microbiol **4:**212–221.
37. **Brenner C, Fuller SR.** 1992. Structural and enzymatic characterization of a purified prohormone-processing enzyme: secreted, soluble Kex2 protease. Proc Natl Acad Sci U S A **89:**922–926. http://dx.doi.org/10.1073/pnas.89.3.922.
38. **Gonzalez-Perez D, Garcia-Ruiz E, Alcalde M.** 2012. *Saccharomyces cerevisiae* in directed evolution: an efficient tool to improve enzymes. Bioengineered **3:**1–6. http://dx.doi.org/10.4161/bbug.3.1.19011.
39. **Cortassa S, Aon JC, Aon MA.** 1995. Fluxes of carbon, phosphorylation, and redox intermediates during growth of *Saccharomyces cerevisiae* on different carbon-sources. Biotechnol Bioeng **47:**193–208. http://dx.doi.org/10.1002/bit.260470211.
40. **Mate D, Garcia-Ruiz E, Camarero S, Shubin V, Falk M, Shleev S, Alcalde M.** 2013. Switching from blue to yellow: altering the spectral properties of a high redox potential laccase by directed evolution. Biocatal Biotransformation **31:**8–21. http://dx.doi.org/10.3109/10242422.2012.749463.
41. **Brake AJ.** 1990. α-Factor leader-directed secretion of heterologous proteins from yeast. Methods Enzymol **185:**408–421. http://dx.doi.org/10.1016/0076-6879(90)85036-N.
42. **Dym O, Eisenberg D.** 2001. Sequence-structure analysis of FAD-containing proteins. Protein Sci **10:**1712–1728. http://dx.doi.org/10.1110/ps.12801.
43. **Zu Z, Wang J, Zhou N, Zhao C, Qiu J.** 2013. A highly sensitive method for quantitative determination of L-amino acid oxidase activity based on the visualization of ferric-xylenol orange formation. PLoS One **8:**e82483. http://dx.doi.org/10.1371/journal.pone.0082483.
44. **Kumar KA, Reddy TC, Reddy GV, Reddy DBK, Mahipal SVK, Sinha S, Gaikwad AN, Reddanna P.** 2011. High-throughput screening assays for cycloxygenase-2 and 5-lipoxygenase, the targets for inflammatory disorders. Indian J Biochem Biotechnol **48:**256–261.
45. **Lussier M, Sdicu AM, Bussey H.** 1999. The KTR and MNN1 mannosyltransferase families of *Saccharomyces cerevisiae*. Biochim Biophys Acta **1426:**323–334. http://dx.doi.org/10.1016/S0304-4165(98)00133-0.
46. **Khersonsky O, Rosenblat M, Toker L, Yacobson S, Hugenmatter A, Silman I, Sussman JL, Aviram M, Tawfik D.** 2009. Directed evolution of serum paraoxonase PON3 by family shuffling and ancestor/consensus mutagenesis, and its biochemical characterization. Biochemistry **48:**6644–6654. http://dx.doi.org/10.1021/bi900583y.
47. **Jochens H, Aerts D, Bornscheuer UT.** 2010. Thermostabilization of an

esterase by alignment-guided focused directed evolution. Protein Eng Des Sel **23:**903–909. http://dx.doi.org/10.1093/protein/gzq071.

48. **Zhang ZG, Yi ZL, Pei XQ, Wu ZL.** 2010. Improving the thermostability of *Geobacillus stearothermophilus* xylanase XT6 by directed evolution and site-directed mutagenesis. Bioresour Technol **101:**9272–9278. http://dx.doi.org/10.1016/j.biortech.2010.07.060.
49. **Kiess M, Hecht HJ, Kalisz HM.** 1998. Glucose oxidase from *Penicillium amagasakiense*: primary structure and comparison with other glucose-methanol-choline (GMC) oxidoreductases. Eur J Biochem **252:**90–99.
50. **Shusta EV, Kieke MC, Parke E, Kranz DM, Wittrup KD.** 1999. Yeast polypeptide fusion surface display levels predict thermal stability and soluble secretion efficiency. J Mol Biol **292:**949–956. http://dx.doi.org/10.1006/jmbi.1999.3130.
51. **Böckle B, Martinez MJ, Guillen F, Martinez A.** 1999. Mechanism of peroxidase inactivation in liquid cultures of the ligninolytic fungus *Pleurotus pulmonarius*. Appl Environ Microbiol **65:**923–928.
52. **Peter S, Karich A, Ullrich R, Gröbe G, Scheibner K, Hofrichter M.** 2014. Enzymatic one-pot conversion of cyclohexane into cyclohexanone: comparison of four fungal peroxygenases. J Mol Catal B Enzymol **103:**47–51. http://dx.doi.org/10.1016/j.molcatb.2013.09.016.
53. **Carro J, Ferreira P, Rodriguez L, Prieto A, Serrano A, Balcells B, Arda A, Jimenez-Barbero J, Gutierrez A, Ullrich R, Hofrichter M, Martinez AT.** 2014. 5-Hydroxymethylfurfural conversion by fungal aryl-alcohol oxidase and unspecific peroxygenase. FEBS J http://dx.doi.org/10.1111/febs.13177.
54. **Gonzalez-Perez D, Alcalde M.** 2014. Assembly of evolved ligninolytic genes in *Saccharomyces cerevisiae*. Bioengineered **5:**254–263. http://dx.doi.org/10.4161/bioe.29167.